Giant Stark effect in coupled quantum wells: Analytical model

Thomas Garm Pedersen[*]

Department of Materials and Production, Aalborg University, DK-9220 Aalborg Øst, Denmark

Coupled quantum wells have been proposed as candidates for highly polarizable structures due to their near-degenerate and dipole-coupled electronic states. Hence, many interesting applications in linear and nonlinear optics can be envisioned. We analyze this proposal considering a simple structure with a delta-function barrier separating the wells. While very substantial Stark shifts are certainly predicted for this geometry, perturbative estimates based on polarizabilities (and hyperpolarizabilities) fail beyond a critical field strength that depends inversely on the barrier. Hence, a giant Stark effect due to near-degenerate states is invariably limited by a small critical field. Our analytical (hyper) polarizability expressions are applied to find quantitative Stark shifts for GaAs quantum wells and transition-metal dichalcogenide bilayers. The predicted Stark shifts and critical fields agree with the field dependence observed in a range of available experiments.

I. INTRODUCTION

The Stark effect is a measure of the change in electronic energy levels due to external electric fields. It is essential for several device applications and as a diagnostic tool [1–4]. For these reasons, systematic searches for structures and molecules exhibiting a large Stark effect have been reported [5–9]. Such structures are expected to exhibit large linear and nonlinear optical response due to their large polarizability and hyperpolarizabilities. In weak fields, the response can be understood from the unperturbed [superscript "(0)"] eigenstates $\varphi_n^{(0)}$ and the associated energies $E_n^{(0)}$. Perturbation theory then shows that the contribution to the polarizability of state $\varphi_n^{(0)}$ due to a state $\varphi_m^{(0)}$ is proportional to $|\langle\varphi_m^{(0)}|x|\varphi_n^{(0)}\rangle|^2/(E_m^{(0)} - E_n^{(0)})$, where $\langle\varphi_m^{(0)}|x|\varphi_n^{(0)}\rangle$ is the transition dipole moment. Thus, materials possessing near-degenerate ($E_m^{(0)} \approx E_n^{(0)}$) and dipole-coupled pairs of states are natural candidates for useful materials. Their large response to (weak) electric fields constitutes an example of a "giant" Stark effect [9].

The prototypical example of an electronic system possessing near-degenerate and dipole-coupled states is that of two identical coupled quantum wells [9–17] as illustrated in Fig. 1(a). Physically, such quantum wells may be formed by semiconductor heterostructures [10–17] that are usually modeled as one-dimensional square-well potentials. However, similar physics is found in coupled quantum dots [18] and "molecular" systems such as ladder polymers [19] or transition-metal dichalcogenide (TMD) bilayers [20–24]. If the barrier between the wells is properly adjusted, the ground state $\varphi_1^{(0)}$ and first excited state $\varphi_2^{(0)}$ will be close in energy but still dipole coupled. A large barrier reduces the energy difference $E_2^{(0)} - E_1^{(0)}$ and may lead to a large polarizability. In a perfectly symmetric structure, the unperturbed ground and excited states are even and odd superpositions of localized states pertaining to the individual wells. In quantum-chemistry

language, these are bonding and antibonding combinations of "atomic" orbitals. In an electric field above a certain critical strength, however, the ground and first excited states become increasingly localized in the left (positively biased) and right (negatively biased) wells, respectively. Hence, the induced dipole moment saturates at a value given by the separation between quantum well centers in this case. Consequently, there are clearly limits to the achievable induced dipole moment. This is essentially a nonperturbative effect and the simple physical picture based on a field-independent polarizability is restricted to fields well below the critical one.

In the present paper, we analyze a simple model of coupled one-dimensional quantum wells separated by a Dirac delta barrier of adjustable height. This system has been studied previously in the absence of fields [25,26]. Hence, in the present work, we expand the model by adding a constant electric field. Such a coupled quantum well structure captures the essential elements of the giant Stark effect. Importantly, however, it may be analyzed analytically even in the presence of arbitrarily strong electric fields. Hence, the exact Stark shift of all states is readily accessible. In addition, polarizabilities α_n and first hyperpolarizabilities β_n of state $\varphi_n^{(0)}$ can be obtained analytically. With this model, we are therefore in a position to analyze (i) the barrier dependence of α_n and β_n and (ii) the limits of the perturbative regime. We restrict the attention to carriers in parabolic bands characterized by an isotropic effective mass. The derived expressions, therefore, apply to both electrons and holes but, for simplicity, electrons will be assumed in all derivations (for holes, the sign of the dipole interaction should simply be inverted). Also, we omit excitonic effects and, hence, consider only single-particle states. We begin this paper by introducing, in Sec. II, the double quantum well model and associated eigenstate problem. This problem is then analyzed using perturbative and nonperturbative approaches in Secs. III and IV, respectively. A comparison of the two is made to illustrate the limits of the perturbative regime. Moreover, numerical estimates are provided and compared to experiments for some characteristic

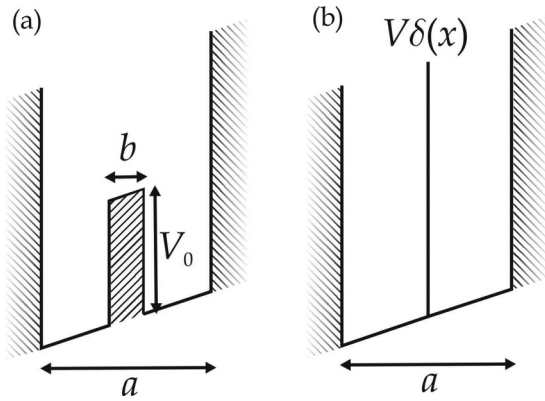_____
[*]tgp@mp.aau.dk

(a) (b) $V\delta(x)$

FIG. 1. Double quantum well with total width a modeled with a finite interwell barrier (a) and a delta-function barrier (b). The potential is tilted by the electric field.

realizations of double-well structures in Sec. V. Finally, a summary is given in Sec. VI.

II. STARK EFFECT

The applied model including the electric field is illustrated in Fig. 1. We consider a one-dimensional double quantum well with a full width a and infinite outer confinement restricting electrons to move in the range $-a/2 \leqslant x \leqslant a/2$. The two wells are separated by a potential barrier of width b and height V_0. However, to simplify the analysis, we take the limit $b \to 0$ while keeping $V \equiv V_0 b$ finite. Hence, the barrier is modeled as a Dirac delta function $V\delta(x)$ in this limit as shown in Fig. 1(b). The advantages of this simplification are that (i) compact exact results can be found and (ii) the barrier dependence is contained in the single parameter V.

The assumption of infinite outer confinement implies Dirichlet boundary conditions for the wave function $\varphi(x)$ at $x = \pm a/2$. It is convenient to use units, in which $e = \hbar = m_{\text{eff}} = a = 1$ with m_{eff} the effective electron mass. Throughout, we therefore take $\hbar^2/(m_{\text{eff}} a^2)$ as the energy unit and electric fields are measured in units of $\hbar^2/(e m_{\text{eff}} a^3)$. In addition, polarizabilities and hyperpolarizabilities are given in units of $\alpha_0 = e^2 m_{\text{eff}} a^4/\hbar^2$ and $\beta_0 = e^4 m_{\text{eff}}^3 a^{10}/\hbar^6$, respectively. Hence, in the presence of a normalized electric field $\mathcal{E}$, the full eigenvalue problem for electrons is simply

$$\left\{ -\frac{1}{2}\frac{d^2}{dx^2} + V\delta(x) + \mathcal{E}x \right\}\varphi(x) = E\varphi(x), \quad \varphi\left(\pm\frac{1}{2}\right) = 0. \tag{1}$$

The wave function is continuous at the origin but the presence of a delta function implies a discontinuous slope, i.e., $\varphi'(0_+) - \varphi'(0_-) = 2V\varphi(0)$. We will now analyze this problem using both perturbative and nonperturbative approaches.

III. PERTURBATIVE REGIME

We begin by studying the unperturbed ($\mathcal{E} = 0$) states $\varphi_n^{(0)}(x)$ that form the basis for the perturbation expansion. We will restrict ourselves to $V \geqslant 0$ and so the unperturbed energies $E_n^{(0)} \equiv k_n^2/2$ are always positive. The unperturbed eigenstates can be classified as even-parity ($n = 1, 3, 5, \ldots$)
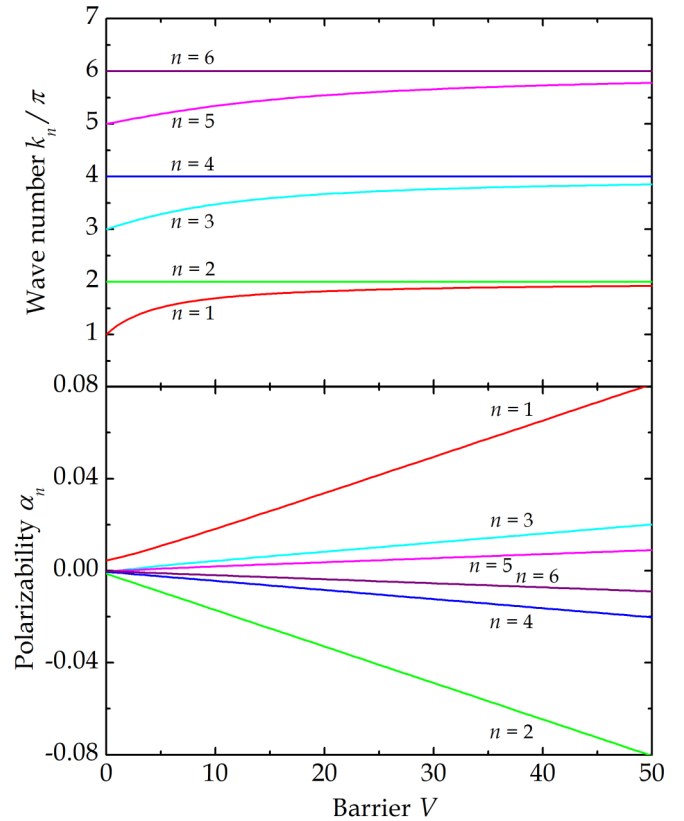

FIG. 2. Barrier dependence of the wave numbers k_n of field-unperturbed states (top panel) and polarizability α_n (lower panel) using the same color code in both panels and with n indicating the state.

states and odd-parity ($n = 2, 4, 6, \ldots$) states. The odd states are particularly simple, since their node at the origin ensures that there is no effect of the delta-function barrier. Hence, for these states $k_n = n\pi$ and $\varphi_n^{(0)}(x) = \sqrt{2}\sin(k_n x)$. The even-parity states are slightly more complicated and can be written as [26]

$$\varphi_n^{(0)}(x) = \left(\frac{2k_n}{k_n - \sin k_n} \right)^{1/2} \sin\left[k_n\left(\frac{1}{2} - |x| \right) \right]. \tag{2}$$

Enforcing the boundary condition connecting the slopes at $x = 0_\pm$ then immediately leads to the eigenvalue condition $V\tan(\frac{1}{2}k_n) + k_n = 0$. For $V = 0$, the solutions are again $k_n = n\pi$, while the wave numbers approach $(n + 1)\pi$ as V increases. A simple expansion shows that, in the limit of large V, $k_n \approx (n + 1)\pi V/(V + 2)$. Hence, any given even-parity state becomes near degenerate with the odd-parity one just above it in this limit. This behavior is illustrated in the top panel of Fig. 2. It may be noted that near degeneracy is reached at low barrier heights for low-lying state pairs, while higher pairs remain energetically separated even in cases of relatively high barriers.

To compute the corrections due to a weak electric field, we write the wave functions as the series $\varphi_n = \varphi_n^{(0)} + \mathcal{E}\varphi_n^{(1)} + \mathcal{E}^2\varphi_n^{(2)} + \cdots$ and, similarly, $E_n = E_n^{(0)} + \mathcal{E}^2 E_n^{(2)} + \mathcal{E}^4 E_n^{(4)} + \cdots$. Note that only even orders appear in the expansion of the energy for a symmetric (unperturbed) system. In turn, the energy corrections provide the (hyper) polarizability

via $E_n^{(2)} = -\frac{1}{2}\alpha_n$ and $E_n^{(4)} = -\frac{1}{4}\beta_n$. Applying the Dalgarno-Lewis [27–32] technique, we compute the wave-function corrections order by order. For instance, the first-order correction

$\varphi_n^{(1)}$ is found as the solution to the inhomogeneous equation $(H_0 - E_n^{(0)})\varphi_n^{(1)} + x\varphi_n^{(0)} = 0$, where $H_0 = -\frac{1}{2}d^2/dx^2 + V\delta(x)$ is the unperturbed Hamiltonian. Solving, we find

$$\varphi_n^{(1)}(x) = \begin{cases} \dfrac{4x\sin\left(\frac{1}{2}k_n\right)\left\{\sin\left[k_n\left(\frac{1}{2}-|x|\right)\right]+k_n|x|\cos\left[k_n\left(\frac{1}{2}-|x|\right)\right]\right\}-k_n\sin(k_nx)}{4k_n\sin\left(\frac{1}{2}k_n\right)[2k_n(k_n-\sin k_n)]^{1/2}} & \text{even} \\[2ex] \dfrac{1}{4\sqrt{2}k_n^2}\{k_n(1-4x^2)\cos(k_nx) + 4x\sin(k_nx) + V\sin(k_n|x|)\} & \text{odd}. \end{cases} \quad (3)$$

These corrections are plotted in Fig. 3 for small and moderate barriers. Note that parity is switched between $\varphi_n^{(0)}$ and $\varphi_n^{(1)}$. Also, the corrections to the odd states now get an explicit dependence on V. Based on these expressions, the energy correction is $E_n^{(2)} = \langle\varphi_n^{(0)}|x|\varphi_n^{(1)}\rangle$. Accordingly, we find a polarizability $\alpha_n = -2\langle\varphi_n^{(0)}|x|\varphi_n^{(1)}\rangle$ that generally, i.e., for both even and odd states, is given by

$$\alpha_n = \frac{15 - k_n^3\left(1 + \frac{3}{4}(-1)^nV\right)/(k_n - \sin k_n)}{12k_n^4}, \quad (4)$$

which simplifies to $\alpha_n = (15 - k_n^2)/12k_n^4$ if $V = 0$. This agrees with findings in Refs. [28,30–32]. We plot the polarizabilities for a few of the lowest states in the bottom panel of Fig. 2. For all states, α_n varies roughly linearly with V once a threshold of $V \approx 3$ is crossed. The lowest states are the most polarizable ones and moreover, $\alpha_n \approx -\alpha_{n+1}$ for n odd. Hence, if several states are occupied, a large degree of cancellation in the total polarizability will result. Finally, the fact that $|\alpha_n|$ decreases with n derives from the fact that near degeneracy between neighboring states is approached more slowly for high states; cf. the top panel of Fig. 2. The Dalgarno-Lewis approach can be carried to second order to compute the first hyperpolarizability β_n as detailed in the Appendix. The resulting analytical expressions are rather elaborate, in particular, for the even states. However, in all cases, it turns out that β_n varies asymptotically as V^3 for high barriers. Thus, huge values can be expected for weakly coupled quantum well structures.

The extent of the perturbative regime is readily estimated by comparing the separation between unperturbed energies $E_m^{(0)} - E_n^{(0)}$ and the field energy $\sim\mathcal{E}a$. Focusing on the two lowest states and assuming a relatively large barrier, we have $E_2^{(0)} - E_1^{(0)} \approx 8\pi^2/V$ using the asymptotic expression for k_n above. Hence, equating this difference with the field energy leads to a critical field $\mathcal{E}_c^{(1)} \approx 8\pi^2/V$ (recalling that $a = 1$ in our units), above which nonperturbative behavior emerges.

IV. NONPERTURBATIVE REGIME

We now turn to the exact solution for the eigenstates in arbitrary fields. Except for the origin, the perturbed Schrödinger equation, Eq. (1), is essentially Airy's differential equation and general solutions are a combination of first and second Airy functions Ai and Bi. Introducing $z(x) = 2^{1/3}(\mathcal{E}^{1/3}x - \mathcal{E}^{-2/3}E)$ and $z_0 = z(0)$ as well as $z_\pm = z(\pm\frac{1}{2})$ we then find the exact eigenstates:

$$\varphi(x) = C\begin{cases} \{\text{Bi}(z_-)\text{Ai}(z) - \text{Ai}(z_-)\text{Bi}(z)\}/\{\text{Bi}(z_-)\text{Ai}(z_0) - \text{Ai}(z_-)\text{Bi}(z_0)\} & x < 0 \\ \{\text{Bi}(z_+)\text{Ai}(z) - \text{Ai}(z_+)\text{Bi}(z)\}/\{\text{Bi}(z_+)\text{Ai}(z_0) - \text{Ai}(z_+)\text{Bi}(z_0)\} & x > 0 \end{cases}. \quad (5)$$

Here, C is a common normalization factor and the function is continuous at the origin by construction. Matching the two halves using the boundary condition for the slopes at the origin, we find the eigenvalue condition:

$$\text{Ai}(z_-)\text{Bi}(z_+) - \text{Ai}(z_+)\text{Bi}(z_-) = 2^{2/3}\pi\mathcal{E}^{-1/3}V\{\text{Bi}(z_-)\text{Ai}(z_0) - \text{Ai}(z_-)\text{Bi}(z_0)\}\{\text{Bi}(z_+)\text{Ai}(z_0) - \text{Ai}(z_+)\text{Bi}(z_0)\}. \quad (6)$$

As mentioned above, in the absence of a field, the odd-parity eigenstates are completely unaffected by the barrier at the origin due to the node at this position. This is no longer the case in a finite field, however, since states have no definite parity for $\mathcal{E} \neq 0$. This, of course, agrees with the barrier dependence shown for the first-order corrections in Fig. 3.

In Fig. 4, we plot the ground and first excited field-perturbed wave functions from Eq. (5) for vanishing, weak, moderate, and strong fields. First, it is apparent that, in the absence of a field, the first excited state is unaffected by the barrier. Similarly, a low barrier $V = 2$ has only a marginal effect on the excited state in a relatively weak field $\mathcal{E} = 20$. In contrast, a high barrier $V = 20$ means that a field of $\mathcal{E} = 20$ is in the nonperturbative regime, in which ground

and excited states are essentially located in the left and right wells, respectively. As discussed above, the critical field for perturbative behavior with a given (not too small) barrier height is given by $\mathcal{E}_c^{(1)} \approx 8\pi^2/V$, which equates to 39 and 3.9 for $V = 2$ and $V = 20$, respectively. Thus, for $V = 2$, the case $\mathcal{E} = 20$ is still in the perturbative regime while this is not the case for $V = 20$. For sufficiently strong fields and high barriers, a second critical field $\mathcal{E}_c^{(2)}$ is encountered, such that for $\mathcal{E} > \mathcal{E}_c^{(2)}$ both states are located in the left well. This field can be estimated by balancing the orthogonality cost of the excited state (upon moving to the same well as the ground state) with the gain from the electric field. Thus, for high barriers and approximating the eigenstates in each well by sine functions, the energy of the lowest state in the right well
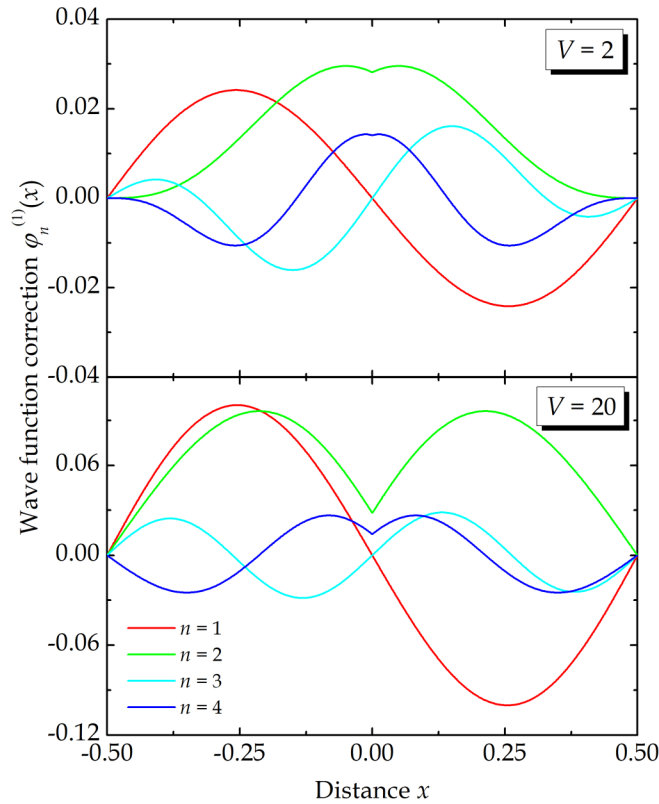
FIG. 3. First-order corrections due to an electric field for wave functions of the four lowest states in structures with small ($V = 2$) and moderate ($V = 20$) barriers.

is $2\pi^2 + \mathcal{E}/4$. Conversely, the second-lowest state in the left well has an energy $8\pi^2 - \mathcal{E}/4$. Balancing these energies leads to a critical field of $\mathcal{E}_c^{(2)} = 12\pi^2 \approx 118$, at which locating both ground and excited states in the left well becomes energetically favorable. Eventually, for $\mathcal{E} \gg \mathcal{E}_c^{(2)}$ there is virtually no effect of the barrier on either state, as shown in the lower panels of Fig. 4.

An illustrative measure of the transition from perturbative to nonperturbative behavior is the induced dipole moment $d_n = \langle \varphi_n | x | \varphi_n \rangle$ of the nth field-perturbed eigenstate. In Fig. 5(a), we plot this measure for ground and excited states for several barriers. The vertical blue lines indicate the critical fields estimated by the formulas explained above. For relatively high barriers and fields above the first critical one, $\mathcal{E}_c^{(1)}$, clear plateaus $d_1 \approx -a/4$ and $d_2 \approx a/4$ are observed for the ground and excited state, respectively. This, then, corresponds to the situation in which these states are located in the left and right wells. Eventually, in very large fields $\mathcal{E} \geqslant 12\pi^2$ and for reasonably high barriers, both states localize in the left well, as discussed above. Note that, interestingly, the transition to this situation is quite abrupt in the high-barrier case.

The induced dipole moments are accompanied by Stark-shifted energies, as shown in Fig. 5(b). In the perturbative regime $\mathcal{E} < \mathcal{E}_c^{(1)}$, the field dependence is approximately quadratic, i.e., $E_n \approx E_n^{(0)} - \frac{1}{2}\alpha_n \mathcal{E}^2$ in terms of the polarizability α_n. Above the critical field, however, the field dependence becomes approximately linear. This corresponds to the behavior of a fixed dipole in the field. For the ground state, the slope approaches $-1/4$ for large barriers corresponding to a state
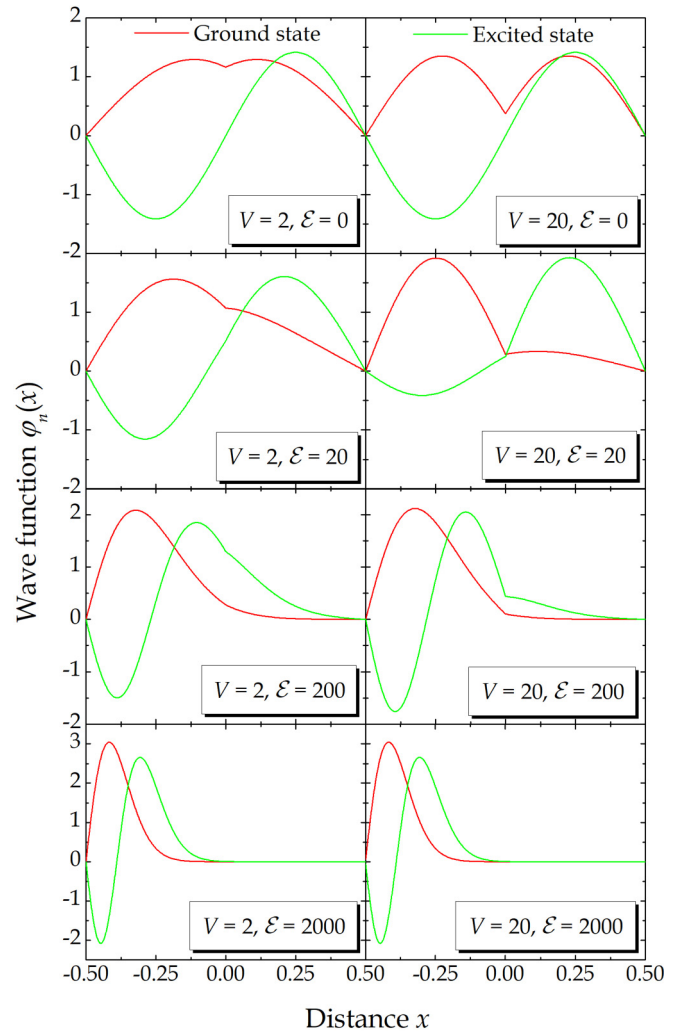

FIG. 4. Ground (red) and first excited (green) states for small ($V = 2$) and large ($V = 20$) barriers in various fields $\mathcal{E} \in [0, 2000]$.

centered at $x = -a/4$. This clearly highlights that the large (quadratic) Stark shifts predicted by the perturbative result $E_n \approx E_n^{(0)} - \frac{1}{2}\alpha_n \mathcal{E}^2$ are limited to low fields and vary much more slowly in strong fields. Again, we emphasize that the critical field defining the upper limit of the perturbative regime is strongly dependent on barrier height, as evidenced by Fig. 5.

We can now make a direct comparison between perturbative and nonperturbative Stark shifts for a number of illustrative cases. To this end, we supplement the second-order perturbation series $E_n \approx E_n^{(0)} - \frac{1}{2}\alpha_n \mathcal{E}^2$ with the fourth-order results $E_n \approx E_n^{(0)} - \frac{1}{2}\alpha_n \mathcal{E}^2 - \frac{1}{4}\beta_n \mathcal{E}^4$ based on hyperpolarizabilities β_n derived in the Appendix. We obviously expect the more accurate fourth-order series to extend the range of the perturbative regime. As will be demonstrated below, though, the fourth-order approximation is vastly more inaccurate than second-order results in the nonperturbative regime. In Fig. 6, perturbative and exact Stark-shifted energies are compared for cases ranging from the barrierless one to very high barriers, $V = 200$. For vanishing and low barriers, the hyperpolarizability correction clearly improves the agreement in the vicinity of the first critical field. For slightly larger fields, however, the correction is strongly overestimated and,
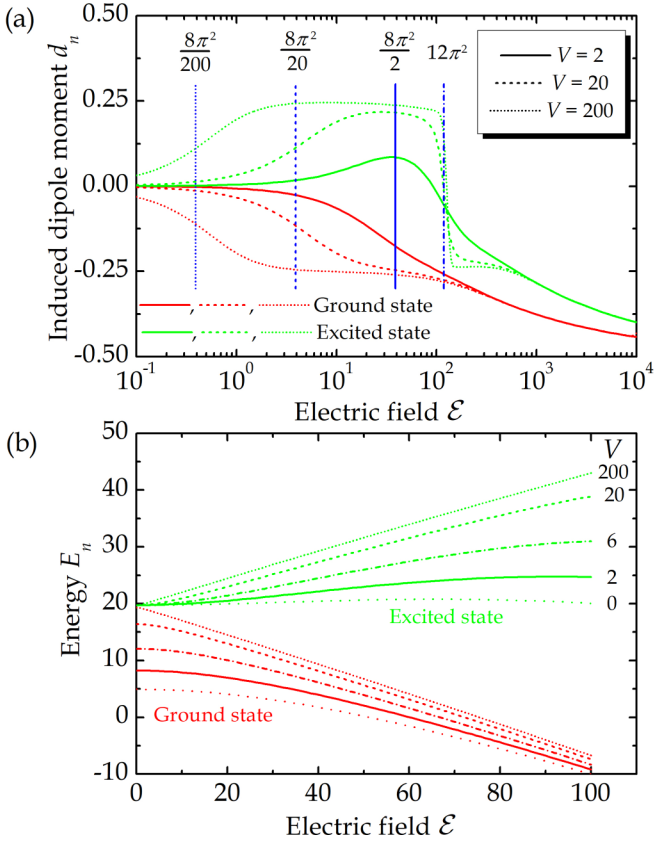
FIG. 5. Electric field dependence of the induced dipole moment (a) and energy (b) for ground (red lines) and first excited (green lines) states. In (a,b), various barrier heights are indicated by line type. The vertical blue lines in (a) indicate first $\mathcal{E}_c^{(1)} = 8\pi^2/V$ and second $\mathcal{E}_c^{(2)} = 12\pi^2$ critical fields.

in fact, the second-order series is more accurate. For $V = 200$, both perturbative series are completely inadequate for $\mathcal{E} > 2$.

It is interesting to apply the recently developed hypergeometric resummation technique [33–35] to the present case in order to find energy expressions valid for arbitrary fields, as demonstrated for TMD excitons [34] and quantum dots [36], as well as low- and three-dimensional hydrogen [33,35]. This approach requires access to at least four terms in the low- and/or high-field perturbative series. Here, we will try to construct a hypergeometric fit to the field dependence of the ground-state energy in order to circumvent the inherent limitations of the simple perturbative series. In brief, in its simplest form [33], one writes the field-dependent energy as the ansatz $E_H(\mathcal{E}) = E_n^{(0)} \times {}_2F_1(h_1, h_2, h_3, -h_4\mathcal{E}^2)$. This expression is guaranteed to agree with the unperturbed result since ${}_2F_1(h_1, h_2, h_3, 0) = 1$. Four constraints are required to uniquely determine the coefficients $h_1 \cdots h_4$. Here, we demand that the low-field Taylor expansion of E_H agree with the fourth-order perturbative series $E_n \approx E_n^{(0)} + \mathcal{E}^2 E_n^{(2)} + \mathcal{E}^4 E_n^{(4)}$. Moreover, for fields approaching $\mathcal{E}_c^{(1)}$, the ground state varies roughly as $E_1 \approx -\frac{1}{4}\mathcal{E}$. Thus, we require that the high-field expansion of E_H agree with this. The linear field dependence in high fields means that $h_1 = -1/2$. In addition, the low-field constraints are fulfilled provided $2h_3 E_n^{(2)} = h_2 h_4 E_n^{(0)}$ and $-8h_3(1 + h_3)E_n^{(4)} = h_2(1 + h_2)h_4^2 E_n^{(0)}$. Finally, the requirement of a high-field slope of $-\frac{1}{4}$ leads
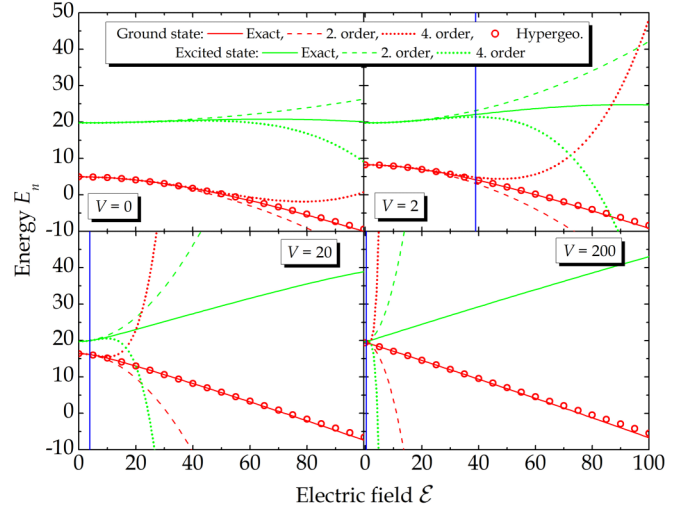

FIG. 6. Comparison of exact (solid line) energies with second- (dashed) and fourth- (dots) order perturbative expansions for ground and first excited state for four different barriers $V = 0$, 2, 20, and 200. The circles show the hypergeometric fit and first critical fields are shown as vertical blue lines.

to $E_n^{(0)}\sqrt{h_4}\Gamma(h_2 + \frac{1}{2})\Gamma(h_3) = -\frac{1}{4}\Gamma(h_2)\Gamma(h_3 + \frac{1}{2})$. Isolating, one readily derives a single equation for h_2, which must subsequently be solved numerically. The assumption of infinite outer confinement means that field-assisted tunneling out of the structure is impossible. Consequently, the coefficient h_4 must be positive [33,36]. Finite barriers, on the other hand, allow for tunneling [34,37] and this is captured by a negative h_4 in the hypergeometric ansatz [33].

We have applied the hypergeometric ansatz to the ground state for various barrier heights. The resulting fits are shown as the circles in Fig. 6. Clearly, the ansatz is an excellent approximation in weak and moderate fields. It outperforms both second- and fourth-order perturbation series and remains highly accurate even in fields larger than the first critical one $\mathcal{E}_c^{(1)}$. Only in high-barrier cases and for fields $\mathcal{E} \gg \mathcal{E}_c^{(1)}$ is it noted that the ansatz lies slightly above the numerically exact results. Thus, we conclude that, similarly to the case of quantum dots [36], the hypergeometric resummation approach incorporating both low- and high-field information is an accurate tool for compact estimates of the Stark shift in coupled quantum wells.

V. DISCUSSION

To convert the universal results of this paper to specific predictions for actual electronic structures, we now aim to obtain conversion factors for two prototypical double quantum well structures: GaAs/Al$_x$Ga$_{1-x}$As heterostructures and MoS$_2$ bilayers. In the former case, GaAs wells are separated by Al$_x$Ga$_{1-x}$As ($x \approx 0.3$) barriers with conduction and valence band offsets $V_0^{(c)} \approx 0.243$ eV and $V_0^{(v)} \approx 0.131$ eV, respectively, assuming a 65:35 ratio between offsets [38]. When constants are reinstated, the dimensionless barrier V is given by $V = V_0 m_{\text{eff}} ab/\hbar^2$ and the first critical field expressed in physical units is $\mathcal{E}_c^{(1)} \approx 8\pi^2\hbar^2/(em_{\text{eff}}a^3V)$. For conduction electrons in GaAs, the effective mass is $m_e \approx 0.067m_0$ while for heavy holes we take $m_{hh} \approx 0.66m_0$ with m_0 the

TABLE I. Normalized barriers V, polarizabilities α_1, and hyperpolarizabilities β_1, as well as critical fields $\mathcal{E}_c^{(1,2)}$ for the ground state in different coupled quantum well systems. The last column is an estimate of the maximum perturbative Stark shift.

Structure	V	α_1 $[\text{eV(nm/V)}^2]$	β_1 $[\text{eV(nm/V)}^4]$	$\mathcal{E}_c^{(1)}$ $(\text{V}/\mu\text{m})$	$\mathcal{E}_c^{(2)}$ $(\text{V}/\mu\text{m})$	$\frac{1}{2}\alpha_1(\mathcal{E}_c^{(1)})^2$ (meV)
GaAs QW (electron) $a = 103.5$ Å, $b = 11.5$ Å	2.6	76	-40×10^3	31	120	37
GaAs QW (electron) $a = 207$ Å, $b = 23$ Å	10	3.0×10^3	-590×10^6	0.98	15	1.5
GaAs QW (heavy hole) $a = 103.5$ Å, $b = 11.5$ Å	14	2.4×10^3	-1.1×10^9	0.60	12	0.43
GaAs QW (heavy hole) $a = 207$ Å, $b = 23$ Å	54	140×10^3	-54×10^{12}	0.019	1.5	0.025
MoS$_2$ bilayer (electron) $a = 9.2$ Å, $b = 3.1$ Å	14	0.23	-0.14	540	11×10^3	34

free-electron mass [38]. To compare with experiments, we will consider the geometry used in Ref. [10] and take $a = 103.5$ Å and $b = 11.5$ Å for the GaAs/Al$_x$Ga$_{1-x}$As case. In addition, for comparison, a structure with a and b doubled will be studied.

For TMDs, the bilayer dimensions can be estimated from the bulk geometry. Such bulk TMDs may be viewed as material layers separated by vacuum slabs forming the barriers. In the usual AA$'$ stacked 2H form, the c-axis lattice constant (perpendicular to the layers) corresponds to a unit cell containing two monolayers as every second layer is rotated 180°. This unit cell therefore consists of two material slabs and two vacuum slabs. Assuming identical thicknesses of material and vacuum slabs, each of these may be taken as $c/4$. The bilayer considered in the present work is formed by two material layers separated by a single vacuum slab. Hence, for MoS$_2$ with $c \sim 12.29$ Å [39], the full width a and barrier width b can be estimated as 3/4 and 1/4 times c, respectively. Thus, we find roughly $a = 9.2$ Å and $b = 3.1$ Å. It may be noted that a model describing van der Waals heterostructures as homogeneous material slabs separated by vacuum regions has recently successfully explained exciton binding energies in such geometries [40]. For MoS$_2$ and other TMDs, the barrier for conduction band electrons can be estimated as the vacuum level relative to the conduction band minimum, i.e., the electron affinity $V_0 \approx 3.8$ eV [41]. In addition, for motion of electrons or holes perpendicular to the layers in atomically thin TMDs it seems appropriate to use $m_{\text{eff}} \approx m_0$. This is in contrast to the in-plane motion within TMD slabs, in which electrons see a fully periodic potential. Hence, for in-plane motion, the effective mass in TMDs is substantially reduced compared to the free-electron value (typically $m_{\text{eff, in-plane}} \sim 0.5m_0$ [41]). For out-of-plane motion in a few-layer geometry, the mass correction is much smaller. For instance, in Ref. [42], an *ab initio* calculation of valence band quantum well states in few-layer WSe$_2$ could be accurately fitted to an infinite-barrier effective mass model using $m_{\text{eff, out-of-plane}} = 1.08m_0$.

In Table I, results are compiled for narrow and wide GaAs quantum wells as well as MoS$_2$ bilayers as representative of TMD structures in general. We provide numerical values for polarizabilities and hyperpolarizabilities as well as first and second critical fields. Furthermore, the maximal Stark shift in

the perturbative regime estimated as $\frac{1}{2}\alpha_1(\mathcal{E}_c^{(1)})^2$ is evaluated. When increasing the GaAs quantum well dimension from ~ 100 to 200 Å, the normalized barrier increases by a factor of 4. This simply reflects the fact that the characteristic quantization energy $\hbar^2/(m_{\text{eff}}a^2)$ decreases quadratically with dimension. Interestingly, the barrier for TMDs $V \approx 14$ is of comparable magnitude to the GaAs barriers. However, when (hyper) polarizabilities are compared, extremely significant differences become apparent. Hence, the ground-state electron polarizabilities of 100 and 200 Å GaAs quantum wells exceed that of MoS$_2$ bilayers by roughly two and four orders of magnitude, respectively. The corresponding figures for GaAs heavy holes are four and five orders of magnitude. This trend is even more dramatic for β_1, in that the wide GaAs quantum well values for electrons and holes are some nine and 14 orders of magnitude larger, respectively, than the result for MoS$_2$ bilayers. These dramatic figures, however, are countered by closely matching opposite trends in critical fields. Thus, the upper critical field for the perturbative regime $\mathcal{E}_c^{(1)}$ is only 0.98 V/μm for electrons in a 200-Å GaAs quantum well while for heavy holes it is as low as 0.019 V/μm. This should be contrasted with the MoS$_2$ bilayer value, which is a substantial $\mathcal{E}_c^{(1)} \approx 540$ V/μm. The second critical field $\mathcal{E}_c^{(2)}$ follows a similar trend. It may be argued that an appropriate figure of merit is given by the maximum perturbative Stark shift $\frac{1}{2}\alpha_1(\mathcal{E}_c^{(1)})^2$. In terms of this measure, the results of Table I show that the heavy-hole response in GaAs structures has the lowest figures, viz., ~ 0.43 meV (100 Å) and ~ 0.025 meV (200 Å), while the electron responses in TMD bilayers and 100-Å GaAs structures are characterized by similar values, $\frac{1}{2}\alpha_1(\mathcal{E}_c^{(1)})^2 \approx 30 - 40$ meV.

Comparing the present calculations to experiments is complicated by the fact that measurements typically rely on optical absorption or emission, which probes transitions between conduction and valence bands. In addition, excitonic effects may affect the interpretation. If, however, excitonic effects are ignored, the total Stark shift observed is simply the sum of electron and hole shifts [31]. For GaAs, this means that the measured Stark shift in the perturbative regime for an electron–heavy hole transition is completely dominated by the hole contribution due to the different effective masses and the scaling $\alpha_n \propto m_{\text{eff}}$. Inspecting Fig. 3(a) in Ref. [10],

the Stark shift for the lowest nonzero reported field strength $\sim 2.2 \times 10^4$ V/cm = 2.2 V/μm can be estimated as $\Delta E \sim -5$ meV. Converting, this means a polarizability of 2.1×10^3 eV(nm/V)^2 in excellent agreement with the computed heavy-hole polarizability in Table I for the ~ 100-Å GaAs double quantum well. However, since no measurements for smaller field strengths are reported in Ref. [10], it is difficult to judge whether a field of 2.2 V/μm is, indeed, in the perturbative (quadratic) regime. From the critical fields in Table I, this appears to be the case for the electron contribution whereas heavy holes have probably entered the nonperturbative regime. Certainly, for larger fields, a quasilinear Stark shift regime is reached in the measurements [10]. The linear regime is very clearly observed in the experiments reported in Ref. [14] employing a rather wide barrier ($a = 125$ Å, $b = 45$ Å), for which $V \approx 64$. This geometry would correspond to a heavy-hole critical field of $\mathcal{E}_c^{(1)} \approx 0.072$ V/μm that is well below the smallest reported field, 3.2 kV/cm = 0.32 V/μm, in those experiments [14].

The reported experimental TMD data are in similarly good agreement with the present theory. Hence, in Ref. [23], Klein *et al.* report MoS$_2$ bilayer polarizabilities of $\frac{1}{2}\alpha \approx 0.4 \times 10^{-8}$ mD/V equivalent to $\alpha \approx 0.17$ eV(nm/V)^2 in good agreement with the predicted 0.23 eV(nm/V)^2. It should be remembered, however, that the measured value is the combined effect of electron and hole Stark shifts, while the value in Table I is for electrons, with a similar value expected for holes. For bilayer MoS$_2$, the nonperturbative regime has been probed by Chu *et al.* [22]. An approximately linear field dependence is found for the Stark shift observed in both transport and photoluminescence data. A slope of $\sim 2 \times (260 - 275)$ meV(nm/V) is reported, in which the prefactor of 2 corresponds to the estimated out-of-plane dielectric constant [22]. For the $\mathcal{E}_c^{(1)} < \mathcal{E} < \mathcal{E}_c^{(2)}$ regime, the present work predicts a fixed electron-hole dipole $\sim a/4 + a/4$ yielding a Stark-shift slope of $a/2 = 460$ meV(nm/V). Thus, again satisfactory agreement with experiments is noted, in particular, given the uncertainty in the experimental field estimate.

To interpret the main findings and explain the limits of the perturbative regime we approximate $k_1 \approx 2\pi$ as is appropriate for $V \geqslant 10$; cf. Fig. 2. We then have $\alpha_1 \approx V/(8\pi)^2 = 1/(8\mathcal{E}_c^{(1)})$. Thus, we reach the important conclusion that polarizabilities and critical fields are clearly inversely related. The physical explanation for this observation is simple: Raising V means that $E_2^{(0)} - E_1^{(0)}$ decreases, which clearly increases α_1 but, at the same time, puts a severe restriction on the field $\mathcal{E}a < E_2^{(0)} - E_1^{(0)}$ allowed in the perturbative regime. Accordingly, despite appearances, the proposed figure of merit $\frac{1}{2}\alpha_1(\mathcal{E}_c^{(1)})^2 \approx \mathcal{E}_c^{(1)}/16$ really scales linearly with the critical field. Importantly, the rationale for near-degenerate, and thereby highly polarizable, states is problematic because $\frac{1}{2}\alpha_1(\mathcal{E}_c^{(1)})^2$ ends up *inversely proportional* to the barrier V. Thus, increasing V to ensure weak coupling between the halves of the double well is a problematic strategy. It is convenient to reinstate physical constants and we then find

$$\frac{1}{2}\alpha_1\left(\mathcal{E}_c^{(1)}\right)^2 \approx \frac{\pi^2\hbar^4}{2m_{\text{eff}}^2 a^3 b V_0}. \quad (7)$$

It is readily verified that this expression is in good agreement with the exact results in Table I. The barrier dependence

has already been discussed but the resulting scaling of Eq. (7) with effective mass and dimensions derives from an interplay between polarizability $\alpha_1 \propto m_{\text{eff}}^2 a^5 b$ and critical field $\mathcal{E}_c^{(1)} \propto m_{\text{eff}}^{-2} a^{-4} b^{-1}$. The upshot summarized by Eq. (7) is that reducing dimensions a and b while maintaining reasonably low effective masses and barriers should provide good candidates for giant Stark-shift geometries. As a case in point, the large maximal perturbative Stark shift $\frac{1}{2}\alpha_1(\mathcal{E}_c^{(1)})^2 = 34$ meV in TMD bilayers demonstrates that these could be of interest for electro-optic and nonlinear-optical applications. As shown in Table I, a similar value is found for the electron response in narrow GaAs quantum wells. However, in applications based on transitions across the band gap, the GaAs response will likely be limited by the heavy-hole response that will reduce the available perturbative regime.

VI. SUMMARY

In this paper, the rationale for giant Stark effects in structures exhibiting near-degenerate states has been critically examined. Using coupled one-dimensional quantum wells as a test case, analytical perturbative and nonperturbative Stark shifts have been obtained and compared. In particular, analytical expressions for polarizabilities and first hyperpolarizabilities have been obtained for all states. The breakdown of perturbation theory above a critical field strength has been examined and a simple estimate for the critical field has been found. Above the critical field, the observed Stark shift is significantly smaller than the perturbation prediction. The correct high-field behavior has been restored, however, through a hypergeometric ansatz adjusted using both low- and high-field information. Finally, numerical predictions for GaAs double quantum wells and bilayer TMDs have been made and successfully compared to measured Stark shifts.

APPENDIX: FIRST HYPERPOLARIZABILITY

By carrying the Dalgarno-Lewis technique to second order, we find the wave-function correction $\varphi_n^{(2)}$. In practice, this entails solving the inhomogeneous problem $(H_0 - E_n^{(0)})\varphi_n^{(2)} + x\varphi_n^{(1)} - E_n^{(2)}\varphi_n^{(0)} = 0$. Although the result is rather lengthy, this task is readily accomplished using symbolic mathematical software. It is then a simple task to compute the fourth-order energy using

$$E_n^{(4)} = \left\langle \varphi_n^{(2)} \middle| x \middle| \varphi_n^{(1)} \right\rangle - E_n^{(2)}\left[\left\langle \varphi_n^{(2)} \middle| \varphi_n^{(0)} \right\rangle + \left\langle \varphi_n^{(1)} \middle| \varphi_n^{(1)} \right\rangle\right]$$
$$\equiv -\tfrac{1}{4}\beta_n. \quad (A1)$$

Starting from even-parity unperturbed states, the final result is a relatively complicated combination of polynomials and trigonometric factors,

$$\beta_n = \frac{F(k_n)}{73\,728 k_n^{10}(k_n - \sin k_n)^3 \sin^3\left(\frac{1}{2}k_n\right)}, \quad (A2)$$

with

$$
\begin{aligned}
F(k) = {} & 12k(7k^8 - 46k^6 + 12\,420k^4 - 121\,120k^2 - 158\,400)\sin\left(\tfrac{1}{2}k\right) \\
& + 4k(15k^8 + 82k^6 - 14\,916k^4 + 130\,080k^2 - 95\,040)\sin\left(\tfrac{3}{2}k\right) \\
& - 24k(k^8 + 5k^6 - 258k^4 + 1680k^2 - 47\,520)\sin\left(\tfrac{5}{2}k\right) \\
& + 24k(k^6 - 6k^4 + 560k^2 - 15\,840)\sin\left(\tfrac{7}{2}k\right) \\
& + 3(40k^{10} + 31k^8 + 2152k^6 - 34\,400k^4 + 506\,880k^2 + 126\,720)\cos\left(\tfrac{1}{2}k\right) \\
& + 3(8k^{10} - 49k^8 - 2312k^6 + 52\,320k^4 - 760\,320k^2 - 168\,960)\cos\left(\tfrac{3}{2}k\right) \\
& + k^2(51k^6 + 568k^4 - 55\,200k^2 + 760\,320)\cos\left(\tfrac{5}{2}k\right) \\
& + (3k^8 - 88k^6 + 1440k^4 + 190\,080)\cos\left(\tfrac{7}{2}k\right) - 63\,360\cos\left(\tfrac{9}{2}k\right).
\end{aligned}
\tag{A3}
$$

The odd-parity states, on the other hand, lead to a compact expression:

$$
\beta_n = \frac{3Vk_n^6 + (9V^3 + 45V^2 + 48V - 64)k_n^4 + 480(3V + 28)k_n^2 - 126\,720}{4608k_n^{10}}.
\tag{A4}
$$

In both even and odd cases, the barrierless limit $V = 0$ is the exceedingly simple result

$$
\beta_n = \frac{-k_n^4 + 210k_n^2 - 1980}{72k_n^{10}}.
\tag{A5}
$$

[1] G. U. Bublitz and S. G. Boxer, Annu. Rev. Phys. Chem. **48**, 213 (1997).

[2] T. Takeuchi, C. Wetzel, S. Yamaguchi, H. Sakai, H. Amano, and I. Akasaki, Appl. Phys. Lett. **73**, 1691 (1998).

[3] Y.-H. Kuo, Y. K. Lee, Y. Ge, S. Ren, J. E. Roth, T. I. Kamins, D. A. B. Miller, and J. S. Harris, Nature **437**, 1334 (2005).

[4] F. Wang, J. Shan, M. A. Islam, I. P. Herman, M. Bonn, and T. F. Heinz, Nat. Mater. **5**, 861 (2006).

[5] M. G. Kuzyk, Phys. Rev. Lett. **85**, 1218 (2000).

[6] M. Ghosh, R. K. Hazra, and S. P. Bhattacharyya, Chem. Phys. Lett. **405**, 410 (2005).

[7] J. Zhou, U. B. Szafruga, D. S. Watkins, and M. G. Kuzyk, Phys. Rev. A **76**, 053831 (2007).

[8] T. J. Atherton, J. Lesnefsky, G. A. Wiggers, and R. G. Petschek, J. Opt. Soc. Am. B **29**, 513 (2012).

[9] E. Crowell and M. Kuzyk, J. Opt. Soc. Am. B **35**, 2412 (2018).

[10] M. N. Islam, R. L. Hillman, D. A. B. Miller, and D. S. Chemla, Appl. Phys. Lett. **50**, 1098 (1987).

[11] Y. J. Chen, E. S. Koteles, B. S. Elman, and C. A. Armiento, Phys. Rev. B **36**, 4562 (1987).

[12] S. R. Andrews, C. M. Murray, R. A. Davies, and T. M. Kerr, Phys. Rev. B **37**, 8198 (1988).

[13] C. C. Phillips, R. Eccleston, and S. R. Andrews, Phys. Rev. B **40**, 9760 (1989).

[14] K. J. Kuhn, C. Juang, and R. B. Darling, J. Appl. Phys. **69**, 3135 (1991).

[15] M. M. Dignam and J. E. Sipe, Phys. Rev. B **43**, 4084 (1991).

[16] F. Capasso, C. Sirtori, and A.Y. Cho, IEEE J. Quantum Electron. **30**, 1313 (1994).

[17] K. Sivalertporn, L. Mouchliadis, A. L. Ivanov, R. Philp, and E. A. Muljarov, Phys. Rev. B **85**, 045207 (2012).

[18] S. Ramanathan, G. Petersen, K. Wijesundara, R. Thota, E. A. Stinaff, M. L. Kerfoot, M. Scheibner, A. S. Bracker, and D. Gammon, Appl. Phys. Lett. **102**, 213101 (2013).

[19] A. Pramanik and H. S. Kang, J. Chem. Phys. **134**, 094702 (2011).

[20] A. Ramasubramaniam, D. Naveh, and E. Towe, Phys. Rev. B **84**, 205325 (2011).

[21] Q. Liu, L. Li, Y. Li, Z. Gao, Z. Chen, and J. Lu, J. Phys. Chem. C **116**, 21556 (2012).

[22] T. Chu, H. Ilatikhameneh, G. Klimeck, R. Rahman, and Z. Chen, Nano Lett. **15**, 8000 (2015).

[23] J. Klein, J. Wierzbowski, A. Regler, J. Becker, F. Heimbach, K. Müller, M. Kaniber, and J. J. Finley, Nano. Lett. **16**, 1554 (2016).

[24] F. Vialla, M. Danovich, D. Ruiz-Tijerina, M. Massicotte, P. Schmidt, T. Taniguchi, K. Watanabe, R. J. Hunt, M. Szyniszewski, N. Drummond, T. G. Pedersen, V. Fal'ko, and F. Koppens, 2D Mater. **6**, 035032 (2019).

[25] I. R. Lapidus, Am. J. Phys. **55**, 172 (1987).

[26] G. A. Vugalter, A. K. Das, and V. A. Sorokin, Phys. Rev. A **66**, 012104 (2002).

[27] A. Dalgarno and J. T. Lewis, Proc. R. Soc. London, Ser. A **233**, 70 (1955).

[28] H. A. Mavromatis, Am. J. Phys. **59**, 738 (1991).

[29] T. G. Pedersen, Solid State Commun. **141**, 569 (2007).

[30] M. A. Maize, M. A. Antonacci, and F. Marsiglio, Am. J. Phys. **79**, 222 (2011).

[31] T. G. Pedersen, Phys. Rev. B **94**, 125424 (2016).

[32] T. G. Pedersen, New J. Phys. **19**, 043011 (2017).

[33] H. Mera, T. G. Pedersen, and B. K. Nikolić, Phys. Rev. Lett. **115**, 143001 (2015).

[34] T. G. Pedersen, S. Latini, K. S. Thygesen, H. Mera, and B. K. Nikolić, New J. Phys. **18**, 073043 (2016).

[35] T. G. Pedersen, H. Mera, and B. K. Nikolić, Phys. Rev. A **93**, 013409 (2016).

[36] T. G. Pedersen, Phys. Rev. A **99**, 063410 (2019).

[37] M. Massicotte, F. Vialla, P. Schmidt, M. Lundeberg, S. Latini, S. Haastrup, M. Danovich, D. Davydovskaya, K. Watanabe,

T. Taniguchi, V. Fal'ko, K. Thygesen, T. G. Pedersen, and F. H. L. Koppens, Nat. Commun. **9**, 1633 (2018).

[38] P. K. Basu, *Theory of Optical Processes in Semiconductors* (Oxford University Press, Oxford, 1997).

[39] J. He, K. Hummer, and C. Franchini, Phys. Rev. B **89**, 075409 (2014).

[40] P. Merkl, F. Mooshammer, P. Steinleitner, A. Girnghuber, K.-Q. Lin, P. Nagler, J. Holler, C. Schüller, J. M. Lupton, T. Korn, S. Ovesen, S. Brem, E. Malic, and R. Huber, Nat. Mater. **18**, 691 (2019).

[41] F. A. Rasmussen and K. S. Thygesen, J. Phys. Chem. C **119**, 13169 (2015).

[42] P. Schmidt, F. Vialla, S. Latini, M. Massicotte, K. Tielrooij, S. Mastel, G. Navickaite, M. Danovich, D. A. Ruiz-Tijerina, C. Yelgel, V. Fal'ko, K. S. Thygesen, R. Hillenbrand, and F. H. L. Koppens, Nat. Nanotechnol. **13**, 1035 (2018).